Appl. Phys. A 69 [Suppl.], S45–S48 (1999) / Digital Object Identifier (DOI) 10.1007/s003399900178

Applied Physics A
Materials
Science & Processing

Pulsed laser deposition

D. Bäuerle, R. Rössler, J. Pedarnig, S.H. Yun, R. Dinu, N. Arnold

Angewandte Physik, Johannes-Kepler-Universität Linz, A-4040 Linz, Austria

Received: 9 August 1999/Accepted: 11 August 1999/Published online: 28 December 1999

Abstract. In this paper we discuss some fundamentals on uniform target ablation and present some new results on thin films of high-temperature superconductors, ferroelectrics, and polymers.

PACS: 73.50.-h; 81.15.Fg; 68.60.-p

Pulsed laser deposition (PLD) has become a popular technique for the fabrication of thin films of multicomponent materials. Among the materials studied in most detail are high-temperature superconductors, compound semiconductors, dielectrics, ferroelectrics, electrooptic and giant magnetoresistance oxides, polymers, and various types of heterostructures [1]. PLD is very reliable, offers great experimental versatility, and is fairly simple and fast – as long as small-area films of up to several square centimeters are to be fabricated. With many materials, thin films can be fabricated without the use of corrosive and/or hazardous chemicals. The short turn-around times enable one to efficiently study a great variety of different compounds and film dopings. For these reasons, PLD is particularly suitable in materials research and development. The short interaction times and the strong non-equilibrium conditions in PLD allow, however, some *unique* applications. Among those are *metastable* materials that cannot be synthesized by standard techniques, and the fabrication of films from species, clusters or fragments that are generated only during pulsed laser ablation. With certain systems, the physical properties of such films are superior to those fabricated by standard evaporation, electron-beam evaporation, etc.

Epitaxial and large-grain oriented films are fabricated by ablating the target material in either vacuum or an inert or reactive atmosphere at pressures of about 0.01 and a few mbar. In this regime, the films are synthesized primarily from a flux of atoms/ions and small molecules impinging onto the substrate surface. The situation changes significantly with higher gas pressures that are, typically, within the range of 1 to several hundred mbar. Such conditions favor vapor-phase condensation and the formation of clusters and nanocrystals. The latter have diameters of, typically, 1 to 20 nm and contain 10^2 to 10^6 atoms. By condensing the nanoparticles onto a substrate, nanocrystalline or cluster-assembled films have been fabricated. Nanocrystalline films have physical properties that are quite different from epitaxial or large-grain polycrystalline films. They may show quantum confinement effects or may consist of entirely new composite materials formed, e.g., in a reactive atmosphere [2–5].

We discuss some fundamentals of uniform target ablation and concentrate on new results on thin films of high-temperature superconductors, ferroelectrics, and polymers.

1 Homogeneous target ablation

Pulsed laser deposition of uniform films with low particulate densities requires the suppression of cone formation and uniform target ablation. Optimal conditions are achieved when the target is rotated and simultaneously translated. The frequencies of rotation, ω_r, and translation, ω_t, and laser-pulse repetition, ω_l, must all be incommensurate. The target must be moved symmetrically to the fixed laser beam. If the radius of the laser beam is very small compared to the radius of the target, i.e. if $w \ll R_t$, the temporal dependence of the translational motion along the diameter of the target, say in the x direction, must follow a square-root dependence:

$$x = \sqrt{2} R_t \left(\left| \frac{2t}{T_t} - \left[\frac{2t}{T_t} \right] \right| \right)^{1/2} \operatorname{sign} \left(\frac{t}{T_t} - \left[\frac{t}{T_t} \right] \right) . \qquad (1)$$

The square brackets indicate that the round value, i.e., the integer closest to a given value should be taken. R_t is the amplitude of the target oscillations in the x direction. Figure 1 shows the average exposure as a function of the normalized distance from the target center, ϱ/R_t, for four different beam shapes. The most uniform exposure of targets is achieved with top-hat circular beams of radii $w \lesssim 0.1 R_t$ (*full curve*). A nonlinear dependence of the ablation rate on intensity will *sharpen* the interaction zone and thereby diminish nonuniformities in the ablation related to the finite size of the laser beam [6].

COLA'99 – 5th International Conference on Laser Ablation, July 19–23, 1999 in Göttingen, Germany

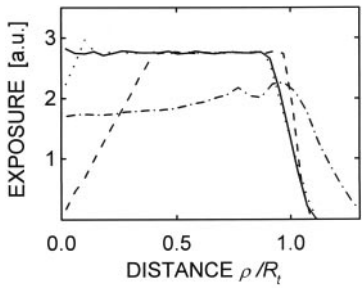

Fig. 1. Dependence of the (average) target exposure on the (dimensionless) distance from the target center, ϱ/R_t. In all cases, the ratio of frequencies is $\omega_\mathrm{l} : \omega_\mathrm{r} : \omega_\mathrm{t} = 10e : \pi : 1$. The different beam shapes employed have the *same* total power. $2w_x$ and $2w_y$ are the size of the laser beam in x and y directions, respectively. *Solid curve*: top-hat circular beam with $w_x = w_y = 0.1\,R_\mathrm{t}$; beam center at $\boldsymbol{b} = (0, 0)$. *Dotted curve*: top-hat square beam with $w_x = w_y = 0.1\,R_\mathrm{t}$, $\boldsymbol{b} = (0, 0)$. *Dashed curve*: thin vertical top-hat rectangular beam with $w_x = 0.01\,R_\mathrm{t}$, $w_y = 0.2\,R_\mathrm{t}$, $\boldsymbol{b} = (0, 0.2\,R_\mathrm{t})$. *Dash-dotted curve*: top-hat rectangular beam with $w_x = 0.1\,R_\mathrm{t}$, $w_y = 0.4\,R_\mathrm{t}$, $\boldsymbol{b} = (0, 0.4\,R_\mathrm{t})$ and *sinusoidal* translational motion (after [6])

2 High-temperature superconductors

Almost all high-temperature superconductors (HTS) have been fabricated by PLD as epitaxial or large-grain oriented thin films [1]: $REBa_2Cu_3O_{7-\delta}$ (RE = rare earth) and $REBaSrCu_3O_{7-\delta}$ including *c*-axis-oriented metastable $LuBa_2Cu_3O_{7-\delta}$, $LuBaSrCu_3O_{7-\delta}$, and $TmBaSrCu_3O_{7-\delta}$ [7], different phases of $Bi_2Sr_2Ca_{n-1}Cu_nO_{2(n+2)\pm\delta}$ $T_{c0} \lesssim 10\,\mathrm{K}$ $(n = 1)$; $86\,\mathrm{K}$ $(n = 2)$; $110\,\mathrm{K}$ $(n = 3)$] [8], $Tl_2Ba_2Ca_{n-1}Cu_nO_{2(n+2)\pm\delta}$ [$T_{c0} = 95\,\mathrm{K}$ $(n = 1)$, 110 K(n=2), $125\,\mathrm{K}$ $(n = 3)$] [9], and $HgBa_2Ca_{n-1}Cu_nO_{2(n+1)\pm\delta}$ [$T_{c0} = 95\,\mathrm{K}$ $(n = 1)$; $124\,\mathrm{K}$ $(n = 2)$; $134\,\mathrm{K}$ $(n = 3)$] [10, 11].

The physical properties of HTS are strongly anisotropic and cannot be fully determined from epitaxial films. Also, these materials are often not available as single crystals. In this situation it has been found useful to fabricate films on off-axis-oriented substrates.

2.1 Films with step-like morphology

The growth of films with step-like morphology has been demonstrated for YBCO, Bi-2212, and Hg-1212 on off-*c*-axis-oriented (001) $SrTiO_3$ substrates (Fig. 2). The *c* axis of such films is tilted by $0 \le \theta_f \le 2°$ with respect to the (001) direction of the substrate, which itself forms an angle θ_s with the surface normal $\hat{n}$. The step-like structure of the films permits one to investigate the strongly anisotropic properties of these materials. For example, the resistance along the projection of the *c* axis onto the film surface is given by

$$R_c \approx \frac{l}{A}\left(\varrho_{ab}\cos^2\theta_\mathrm{s} + \varrho_c \sin^2\theta_\mathrm{s}\right) . \qquad (2)$$

In the perpendicular direction we have

$$R_{ab} = \frac{l}{A}\varrho_{ab} . \qquad (3)$$

The resistivities ϱ_{ab} and ϱ_c derived in this way are plotted in Fig. 3 for Bi-2212 films on vicinal $SrTiO_3$ substrates for various tilt angles θ_s and different film thicknesses. With tilt angles $\theta_\mathrm{s} > 15°$ the quality of the films starts to deteriorate

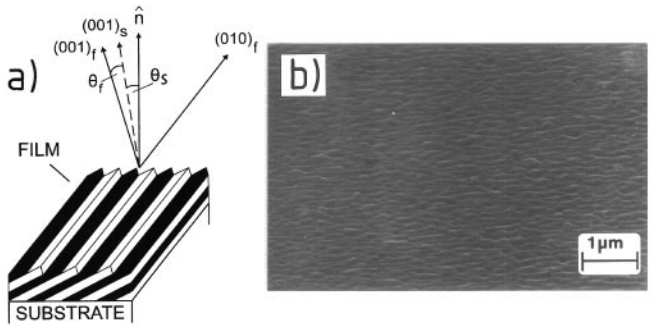

Fig. 2. **a** Schematic picture which shows an off-*c*-axis-oriented (001) $SrTiO_3$ or MgO substrate (surface normal $\hat{n}$) and a step-like-grown film. The angle between $\hat{n}$ and the (001) direction of the substrate is θ_s. The angle between the *c* axis of the film and the substrate is $0 \le \theta_\mathrm{f} \le 2°$. **b** SEM picture of a Bi-2212 film on a $SrTiO_3$ substrate with $\theta_\mathrm{s} = 10°$ (after [7])

as a result of mixed growth in the *c* and *ab* directions. This is reflected in the drop-off in ϱ_c. With angles $\theta_\mathrm{s} \le 15°$ the values of ϱ_c and ϱ_{ab} are *independent* of the film thickness h_1, except for the thinnest film where inhomogeneities in h_1 become important. A further point is the systematic difference in ϱ_c values between the two pictures. This is probably related to the $SrTiO_3$ substrates. For the $\varrho(\theta_\mathrm{s})$ and $\varrho(h_1)$ investigations, we employed substrates that were supplied from Kelpin and CrysTec, respectively. The initial results obtained with Hg-1212 films grown on vicinal (001) $SrTiO_3$ substrates with $\theta_\mathrm{s} = 10°$ are shown in Fig. 4. The anisotropy in electrical resistivities derived from resistance measurements according to (2) and (3) is $\varrho_c(300\,\mathrm{K})/\varrho_{ab}(300\,\mathrm{K}) \approx 684$ [11].

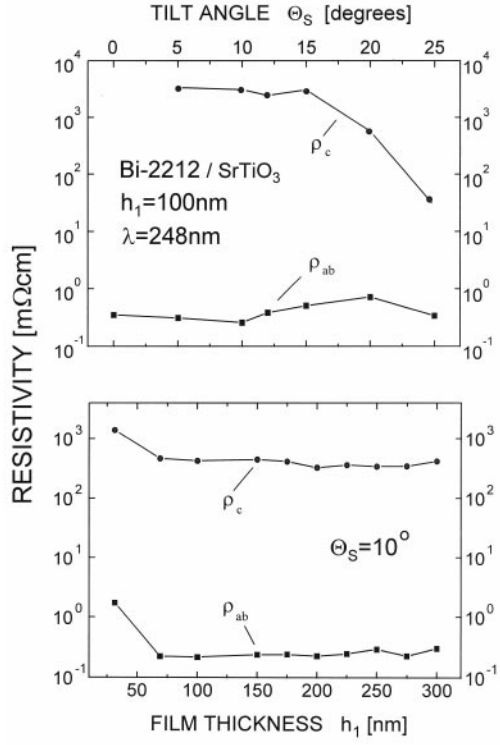

Fig. 3. Electrical resistivities ϱ_{ab} and ϱ_c of Bi-2212 films deposited by PLD on vicinal $SrTiO_3$ substrates

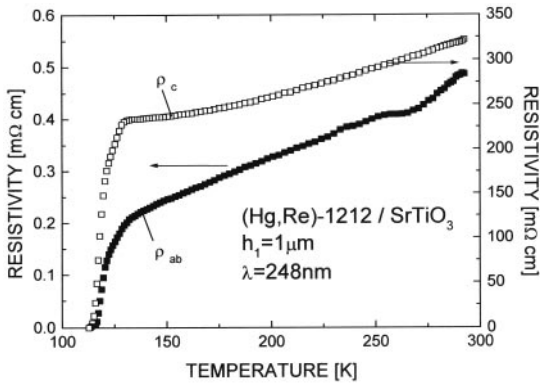

Fig. 4. (Hg,Re)-1212 film grown on vicinal (001) $SrTiO_3$ with $\theta_s = 10°$. The anisotropy in electrical resistivities is $\varrho_c(300\,\mathrm{K})/\varrho_{ab}(300\,\mathrm{K}) \approx 684$

3 Ferroelectric films

Among the ferroelectric films fabricated by PLD are oxidic perovskites such as $BaTiO_3$, $KTa_{1-x}Nb_xO_3$ (KTN), $PbTi_{1-x}Zr_xO_3$ (PZT) [12], $Pb_{1-y}La_yTi_{1-x}Zr_xO_3$ (PLZT) [13], $Sr_xBa_{1-x}Nb_2O_6$ [14], and incipient ferroelectrics [15] such as $SrTiO_3$ and $KTaO_3$. The perovskite-like materials deposited by PLD include $Bi_4Ti_3O_{12}$ (BTO), $LiNbO_3$, $Pb(Mg_{1/3}Nb_{2/3})O_3$ (PMN) [16], $SrBi_2Ta_2O_9$ (SBT) [17, 18], etc. [1].

One of the most promising compounds for applications as nonvolatile ferroelectric random access memories (RAMs) is SBT. This material shows very small polarization fatigue, low imprint tendency, and low leakage currents. For the fabrication of $SrBi_2Ta_2O_9$ films and $Bi_2O_3/SrBi_2Ta_2O_9/Bi_2O_3$ multilayers on $Pt/Ti/SiO_2$-coated (100) Si substrates, Bi-enriched targets ($SrBi_{2.2}Ta_2O_9$) have been used in order to compensate for the Bi loss during film deposition. The ferroelectric phase with a dominant (115) orientation was obtained at a substrate temperature of $T_s = 750\,°\mathrm{C}$. The formation of the ferroelectric phase was favored at a lower temperature, $T_s = 650\,°\mathrm{C}$, for $Bi_2O_3/SrBi_2Ta_2O_9/Bi_2O_3$ multilayer structures. The SBT films showed hysteresis loops with a maximum remnant polarization of $P_r = 6.5\,\mu\mathrm{C/cm^2}$, and a coercive field of $E_c = 35\,\mathrm{kV/cm}$.

Figure 5 shows the temperature dependence of the dielectric constant of films deposited at three different substrate temperatures. The strength of the dielectric anomaly is largest for films deposited at $T_s = 750\,°\mathrm{C}$. For temperatures well below $T_{max} \equiv T(\varepsilon'_{max})$ the dielectric constant can be described by a Curie–Weiss (CW) law. In the region $\pm 40\,°\mathrm{C}$ around T_{max} we find a relaxor-like behavior. The dependence $\varepsilon'(T)$ can be approximated by $1/\varepsilon' - 1/\varepsilon'_{max} = B(T - T_{max})^m$ with $m = 1$ and $\varepsilon'_{max} \to \infty$ within the CW region and $m = 2$ for the relaxor state. The fit within the range $\pm 40\,°\mathrm{C}$ around T_{max} yields $m = 1.8$ and $m = 2$ for films deposited at $T_s = 700$ and $750\,°\mathrm{C}$, respectively. It confirms the tendency to relaxor-like behavior around T_{max}. At temperatures below $250\,°\mathrm{C}$ the deviation of ε' from the CW fit has been ascribed to domain-wall motions. The SBT films revealed no significant fatigue after 4×10^{10} switching cycles at $120\,°\mathrm{C}$. Domain pinning led to slight fatigue at room temperature. However, recovery of the non-switchable polarization was possible by keeping the film under a field at $90\,°\mathrm{C}$. Leakage currents of $5 \times 10^{-8}\,\mathrm{A/cm^2}$ for fields up to $100\,\mathrm{kV/cm}$ have been determined. This is sufficient for applications in dynamic random access memory devices.

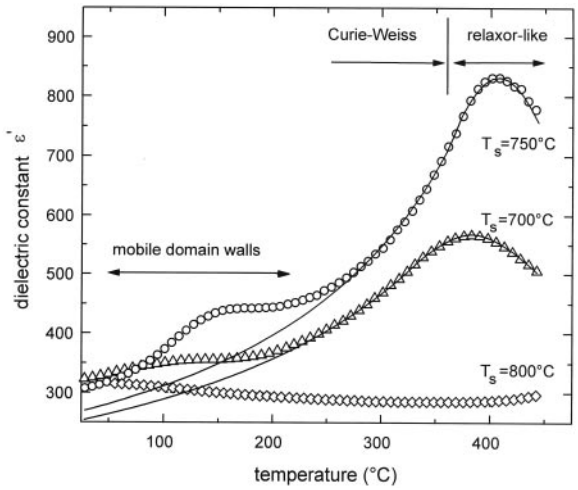

Fig. 5. Dielectric constant ε' versus temperature for $SrBi_2Ta_2O_9$ (SBT) films deposited by 248-nm KrF laser radiation ($\phi \approx 2\,\mathrm{J/cm^2}$) at substrate temperatures $T_s = 750\,°\mathrm{C}$, $700\,°\mathrm{C}$, and $800\,°\mathrm{C}$ in 0.4-mbar O_2 atmosphere. The *full curves* have been calculated, as described in the text (after [17])

4 Teflon (PTFE) films

The good mechanical, thermal, and chemical stability of polytetrafluoroethylene (PTFE) together with its low surface adhesion, frictional resistance, and low dielectric constant makes this material unique for numerous applications in mechanics, microelectronics, chemistry, medicine, and bioscience. For certain applications, it is desirable to fabricate PTFE in the form of thin films.

PTFE films were deposited by means of KrF laser radiation from pressed powder targets (grain sizes 6–9 μm) [19]. The films are highly crystalline, as shown in the optical polarization micrographs of Fig. 6a,b. The size of the spherulites can be enlarged to diameters up to 500 μm by postannealing at 550 °C. The high crystallinity of the PLD-PTFE films has been demonstrated by IR transmission and temperature-dependent dielectric measurements [20]. During film formation, PTFE grains are laser-transferred from

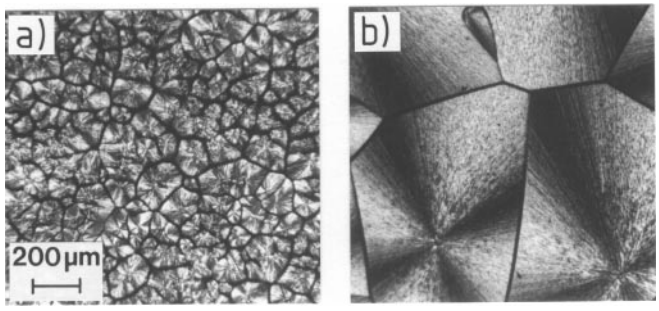

Fig. 6a,b. Optical polarization micrographs showing the surface morphology of KrF-laser-deposited PTFE Teflon films on Si substrates ($\lambda = 248\,\mathrm{nm}$, $\phi = 2.5\,\mathrm{J/cm^2}$, $N_l = 2500$ pulses, 2 Hz). The magnification is the same with both pictures. **a** $T_s = 400\,°\mathrm{C}$. **b** $T_s = 400\,°\mathrm{C}$ and additional postannealing at $T_a = 550\,°\mathrm{C}$ (after [19])

the target to the substrate with subsequent melting and crystallization.

PTFE is well known as an excellent electret (a dielectric exhibiting a quasi-permanent electrical charge). The electret charge may be either a "real" charge or an inherent polarization, or a combination of both. True charge electrets, such as nonpolar PTFE, FEP (tetrafluoroethylene-co-hexafluoropropylene copolymer), and PFA (tetrafluoroethylene-co-perfluoropropoxyethylene) have found widespread applications in acoustic transducers, such as electret microphones [21]. The increasing demand for miniaturized devices makes PTFE films deposited on substrates an interesting charge electret.

The suitability of PLD-PTFE films as charge electrets has been demonstrated by measuring the thermally stimulated voltage decay of corona-charged PLD samples at a rate of 4 °C/min [22]. Figure 7 shows the surface voltage decay of the PLD-PTFE electret. For comparison, data from commercially available PTFE foils are included. Most notable is the excellent temperature-dependent charge stability of PLD-PTFE films with large spherulites, comparable or even better than that of the PTFE foil. Thus, PLD-PTFE films add a new member to the family of "Teflon" materials, interesting for miniaturized electret applications.

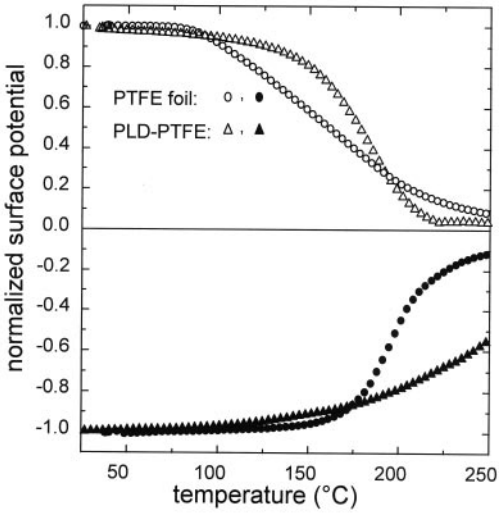

Fig. 7. Thermally stimulated surface potential decay for PTFE foils and PLD-PTFE films with large spherulites (after [22])

References

1. D. Bäuerle: *Laser Processing and Chemistry*, 2nd ed. (Springer, Berlin, Heidelberg 1996) (the third edition will be published in 2000)
2. D.B. Geohegan, A.A. Puretzky, G. Duscher, S.J. Pennycook: Appl. Phys. Lett. **72**, 2987 (1998)
3. W. Marine, B. Luk'yanchuk, M. Sentis: Le VIDE Science, technique et applications, **2**/**4**, 440 (1998)
4. D.H. Lowndes, C.M. Rouleau, T. Thundat, G. Duscher, E.A. Kenik, S.J. Pennycook: Appl. Surf. Sci. **127**-**129**, 355 (1998)
5. R. Serna, T. Missana, C.N. Afonso, J.M. Ballesteros, A.K. Petford-Long, R.C. Doole: Appl. Phys. A **66**, 43 (1998)
6. N. Arnold, D. Bäuerle: Appl. Phys. A **68**, 363 (1999)
7. D. Bäuerle: Supercond. Sci. Technol. **11**, 968 (1998)
8. T. Zahner, R. Stiersdorfer, R. Rössler, J.D. Pedarnig, D. Bäuerle, H. Lengfellner: Physica C **298**, 91 (1998); P. Majewski, R. Nast, F. Aldinger: Supercond. Sci. Technol. **12**, 249 (1999); G. Triscone, M.S. Chae, M.C. de Andrade, M.B. Maple: Physica C **290**, 188 (1997)
9. J.D. O'Connor, D. Dew-Hughes, N. Reschauer, W. Brozio, H.H. Wagner, K.F. Renk, M.J. Goringe, C.R.M. Grovenor, T. Kaiser: Physica C **302**, 277 (1998)
10. W.N. Kang, R.L. Meng, C.W. Chu: Appl. Phys. Lett. **73**, 381 (1998); Y. Morikawi, T. Sugano, A. Tsukamoto, C. Gasser, K. Nakanishi, S. Adachi, K. Tanabe: Physica C **303**, 65 (1998)
11. S.H. Yun, R. Rössler, J. Pedarnig, D. Bäuerle: unpublished
12. Y. Lin, B.R. Zhao, H.B. Peng, B. Xu, H. Chen, F. Wu, H.J. Tao, Z.X. Zhao, J.S. Chen: Appl. Phys. Lett. **73**, 2781 (1998)
13. M. Tyunina, J. Levoska, A. Sternberg, S. Leppävuori: J. Appl. Phys. **84**, 6800 (1998)
14. S.B. Xiong, Z.M. Ye, X.Y. Chen, X.L. Guo, S.N. Zhu, Z.G. Liu, C.Y. Lin, Y.S. Jin: Appl. Phys. A **67**, 313 (1998); M. Nakano, H. Tabata, K. Tanaka, Y. Katayama, T. Kawai: Jpn. J. Appl. Phys. **36**(10A), L1331 (1997)
15. R. Migoni, H. Bilz, D. Bäuerle: Phys. Rev. Lett. **37**, 1155 (1976)
16. J.-P. Maria, W. Hackenberger, S. Trolier-McKinstry: J. Appl. Phys. **84**, 5147 (1998)
17. R. Dinu, M. Dinescu, J.D. Pedarnig, R.A. Gunasekaran, D. Bäuerle, S. Bauer-Gogonea, S. Bauer: Appl. Phys. A **69**, 55 (1999)
18. N. Fujimura, D.T. Thomas, S.K. Streifer, A.I. Kingon: Jpn. J. Appl. Phys. **37**, 5185 (1998)
19. S.T. Li, E. Arenholz, J. Heitz, D. Bäuerle: Appl. Surf. Sci. **125**, 17 (1998)
20. R. Schwödiauer, J. Heitz, E. Arenholz, S. Bauer-Gogonea, S. Bauer, W. Wirges: J. Polym. Sci. B: Polym. Phys. **37**, 2115 (1999)
21. G.M. Sessler: *Electrets*, 3rd ed. Vol. I (Laplacian Press, Morgan Hill 1999)
22. R. Schwödiauer, S. Bauer-Gogonea, S. Bauer, J. Heitz, E. Arenholz, D. Bäuerle: Appl. Phys. Lett. **73**, 2941 (1998)